J. Electrochem. Sci. Eng. **14(5)** (2024) 559-582; http://dx.doi.org/10.5599/jese.1949

Open Access : : ISSN 1847-9286
https://pub.iapchem.org/ojs/index.php/JESE

Original scientific paper

Sealing of cerium oxide coating primers on anodized AA2024-T3 alloy by boiling in Lourier buffers

Stephan Kozhukharov[1,2,✉], Christian Girginov[3], Stefania Portolesi[4], Aleksandar Tsanev[5], Vanya Lilova[2], Mariya Georgieva[6], Emil Lilov[2] and Plamen Petkov[2]

[1]*LAMAR Laboratory for Advanced Materials Research, University of Chemical Technology and Metallurgy, 8 Kliment Ohridski blvd., 1756 Sofia, Bulgaria*
[2]*Department of Physics, University of Chemical Technology and Metallurgy, 8 Kliment Ohridski blvd., 1756 Sofia, Bulgaria*
[3]*Department of Physical Chemistry, University of Chemical Technology and Metallurgy, 8 Kliment Ohridski blvd., 1756 Sofia, Bulgaria*
[4]*University of Calabria, Via Pietro Bucci, 87036 Arcavacata, Cosenza, Italy*
[5]*Institute of General and Inorganic Chemistry, Bulgarian Academy of Sciences, 1113 Sofia, Bulgaria*
[6]*Institute of Mineralogy and Crystallography, Bulgarian Academy of Sciences, 1113 Sofia, Bulgaria*

Corresponding authors: ✉*s.kozhukharov@uctm.edu; Tel.: +359-899-837282; Fax: +359 2 68 54 88*

Received: June 27, 2023; Accepted: July 11, 2024; Published: August 4, 2024

Abstract

*Although their exceptional re-passivation ability, Al-alloys are susceptible to corrosion due to the amphoteric nature of the alumina passivation films. This issue is exacerbated by the disruption of these films by intermetallics on the surfaces of highly doped ones, like AA2024-T3 aircraft alloy. The combination of anodized aluminium oxide (AAO) and cerium conversion coatings (CeCC) shows promise as a coating primer. However, the defective structures of CeO_2 and Al_2O_3 require additional sealing. This research proposes sealing the CeCC/AAO layer by boiling it for 10 minutes in two relatively neutral Lourier buffers, adjusted to pH 7.75, and in a mixture of them. The samples underwent a series of analyses to compare the impact of the sealing procedure on surface topology, properties (*e.g.*, colour and wettability on two samples from each set), and corrosion protective ability. It was assessed after 24 hours of exposure to 3.5 % NaCl model corrosive medium on six samples from each set. The assessments included electrochemical impedance spectroscopy (EIS) and potentiodynamic scanning (PDS) techniques. The results indicate that the borate buffer improves the corrosion protection of the coating primers more effectively than the phosphate and mixed ones.*

Keywords

2024-T3 aluminium alloy; cerium conversion coatings; coating sealing; buffer solutions

Introduction

The use of aluminium alloys as structural materials has significantly increased due to their favourable properties, such as high strength-to-weight ratio, ease of fabrication, high workability, considerable ductility, excellent thermal conductivity, high corrosion resistance, and attractive natural finish [1]. However, despite their exceptional ability to form protective oxide layers, these films have amphoteric properties, making them soluble in both alkaline and acidic media. Their susceptibility to decomposition in Cl^- ions is another major disadvantage of the native oxide layers on aluminium [2-16]. Additionally, intermetallic inclusions on the surface interrupt the integrity of the oxide layer [17], leading to galvanic corrosion [17-21], which can propagate into other forms of localized corrosion [22-28]. These issues necessitate efficient corrosion protection for aluminium-based products, equipment and constructions. Cerium compounds have been increasingly used as environmentally compliant inhibitors [29-43] and advanced protective coating components [44-55]. In particular, cerium conversion coatings (CeCC) have recently been recognized as a promising option for primer layers in advanced multilayered coating systems [56-65]. The CeCC deposition process must include preliminary surface treatment and subsequent CeCC sealing procedures [66-69]. In this sense, anodization is the most appropriate preliminary treatment as it provides an oxide surface suitable for CeCC deposition [70-77]. However, final CeCC layer sealing is essential due to the inherent defectiveness of CeO_2 structures [78-83]. On the basis of the fundamental concepts and recent trends in the formation of advanced multilayered coating systems [60,61,84-86], it can be inferred that CeCC layers deposited after anodization and appropriate CeCC coating primer sealing will be a primary focus for investigation in the coming years. Figure 1 summarizes the main trends in developing advanced multilayered coating systems for effective and reliable corrosion protection of aluminium alloys.

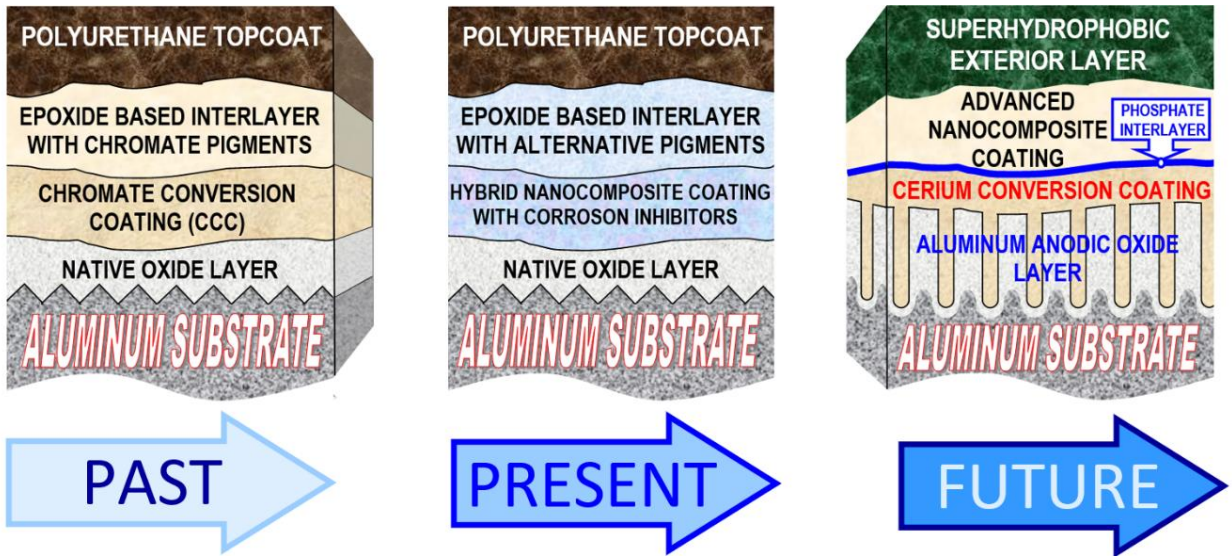

Figure 1. *Trends for elaboration of advanced multilayered coating systems for corrosion protection of aluminium alloys [87,88]*

Phosphate sealing is the most desirable approach for CeCC post-treatment, and optimizing its conditions has been the primary focus of research by Heller *et al.* [89,90] and Andreeva *et al.* [91-93]. This method is also proposed for reliable protection of other metals, demonstrating its versatility [94-98].

Summarizing all aspects related to the development of CeCC layers on preliminary anodized AA2024-T3 aircraft alloy, it was concluded that these layers need additional sealing by suitable

phosphate/borate solutions. The aim of the present research is to determine the effects of boiling CeCC/AAO layers in phosphate, borate, or mixed Lourier buffer solutions with pH 7.75.

Experimental

Sample preparation

Four sets of eight AA2024-T3 samples underwent CeCC/AAO primer layer formation under identical conditions. The layer formation procedures included consecutive preliminary surface treatments, anodization, and cathodic CeCC film formation. Preliminary treatments were conducted in alkaline baths (2 minutes in 50 g dm^{-3} NaOH at 50 °C) and acidic baths (2 minutes in diluted HNO_3 1:1 v/v at 20 °C). Anodization was performed for 15 minutes in 15 wt.% H_2SO_4 at 20 °C. The final cathodic CeCC deposition was carried out for 5 minutes at 5 mA cm^{-2} in a pre-activated CeCC deposition solution under conditions similar to those described in [70,99-102]. The solution composition was 0.025 M $CeCl_3.7H_2O$ combined with 0.025 M $(NH_4)_2Ce(NO_3)_5{\cdot}4H_2O$, with 5 ml of 30 % H_2O_2 activator added to 250 ml of the solution. Each stage was followed by vigorous washing with tap and distilled water without removing the water film prior to CeCC formation.

For this research, the CeCC/AAO-coated AA2024-T3 alloy specimens were divided into four groups: untreated (Ref), boiled for 10 minutes in borate buffer (BB), phosphate buffer (PB), or in a mixed buffer (MB), following the buffer solution preparation procedures proposed by Lourier [103], which were translated into English in previous work [87]. The surface treatment procedures used in the present study are shown in Figure 2.

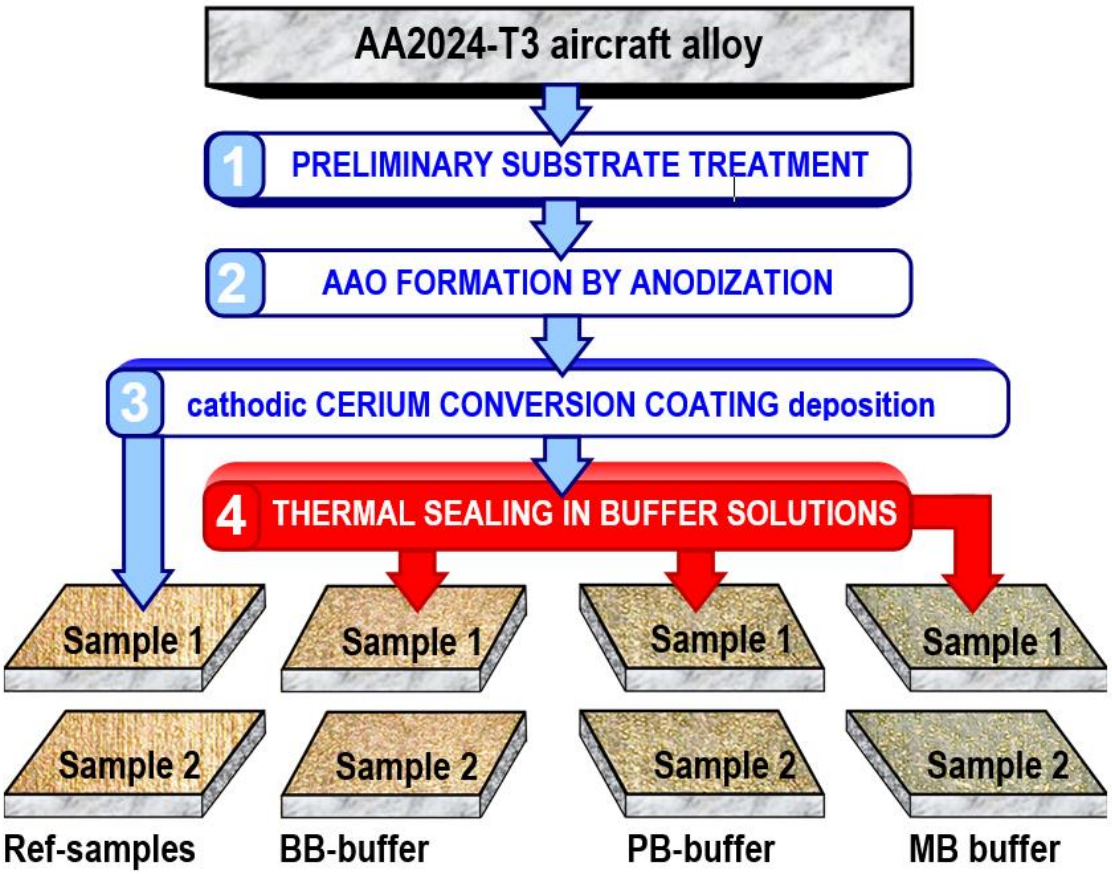

Figure 2. *Sequence of procedures applied for CeCC/AAO coating primed formation and subsequent phosphatation in buffer solutions*

The exact chemical compositions of the buffers used in the present study are shown in Table 1.

Table 1. *Compositions of the used buffer solutions*

Buffer type	Buffer code	Buffer solution compositions		Required volume for 100 ml buffer, cm^3
Borate buffer	BB	First component: $Na_2B_4O_7 \cdot 10H_2O$	19.069 g dm^{-3} solution	52.90
		Second component: HCl	0.100 mol dm^{-3} solution	up to 100
Phosphate buffer	PB	First component: $Na_2HPO_4 \cdot 2H_2O$	11.866 g dm^{-3} solution	92.40
		Second component: KH_2PO_4	9.072 g dm^{-3} solution	up to 100
Mixed buffer	MB	First component: phosphate buffer	(freshly prepared)	50.00
		Second component: borate buffer	(freshly prepared)	up to 100

The buffer compositions in Table 1 were prepared to maintain a relatively neutral medium (pH ≈ 7.75), considering the amphoteric nature of the AAO layer.

Sample analyses

The analyses of all 32 investigated specimens were organized to allow a comparative description of surface properties (colour and wettability), surface topology, and corrosion protection ability.

Two samples from each set underwent surface analyses, while the remaining six samples were subjected only to corrosion tests. Surface properties were characterized by data acquisition from four points on each sample surface, and results were statistically analysed as described in previous work [104].

The respective measurements were performed using an RT 100 Lovibond tintometer and a "Theta Lite" sessile drop tester from Biolin Scientific (UK). The tintometer provided colour characteristics in accordance with the *CIE, L*, a*, b** colour space system, while the sessile drop tester measured the contact angle between the sample surfaces and distilled water drops. The results were statistically analysed following procedures described in previous works [70,99,104,105].

The surface topology of each sample couple was observed using optical metallographic microscopy (OMM). Optical micrographs were acquired at 100× magnification using a Boeco optical microscope equipped with a PK-710G camera from A4Tech, with a resolution of 640×480.

Scanning electron microscopy (SEM) images were obtained from the same sample couples used for surface analyses. Both surface topology and coating thickness were observed at 5000x magnification. All SEM images were obtained using a TESCAN SEM/FIB LYRA I XMU in backscattered electron mode.

To perform a comprehensive comparative analysis, the same sample couples were subjected to X-ray photoelectron spectroscopy (XPS) analysis. XPS studies were conducted using a VG Escalab II system with AlKα radiation at an energy of 1486.6 eV. The chamber pressure was 13.3 MPa. The C1s line of adventitious carbon at 284.6 eV was used as an internal standard to calibrate the binding energies. The photoelectron spectra were corrected by subtracting a Shirley-type background and quantified using the peak area and Scofield's photo-ionization cross-section. The accuracy of the binding energy measurements was ± 0.2 eV.

Corrosion tests

These tests were conducted on the remaining six samples from each set after 24 hours of exposure to a 3.5 % NaCl solution. Electrochemical methods used included electrochemical impedance spectroscopy (EIS) and potentiodynamic scanning (PDS). These methods were performed using an Autolab 30 (Metrohm) equipped with an FRA-2 module. Samples were exposed to the corrosive medium in three-electrode cells, with 0.933 cm^2 of the sample surface as the working electrode, an Ag/AgCl/3 M KCl reference electrode, and a cylindrical platinum mesh counter electrode.

EIS data were recorded at 50 data points from 10 kHz to 0.01 Hz, using excitation signals ranging from 10 to 25 mV relative to the open circuit potential (OCP).

PDS curves were acquired within a potential range from -50 to +500 mV relative to the reference electrode, with a potential sweep rate of 10 mV s^{-1}.

Results and discussion

Among the examined buffer solutions, only the mixed buffer solution (MB) maintained stability, as pH measurements taken 24 hours after boiling showed that the MB solution retained its initial pH value. In contrast, the borate solution precipitated, whereas the phosphate solution became more alkaline, reaching a pH of 8.12.

Prior to assess the barrier properties, two specimens from each set were subjected to topological observations, as mentioned above.

The observed surfaces did not show significant differences, indicating that boiling in buffer solutions does not cause substantial changes in the CeCC/AAO layer morphologies. According to models developed by Nelson *et al.* [106] and Chen *et al.* [107], the CeO_2 phosphating proceeds via monolayer formation due to the highly defective nature of CeO_2 crystal surfaces, as described by various authors [108-112]. Interaction with borate anions will likely also result in the formation of rather thin layers. However, all treated specimens appeared paler, possibly due to the formation of phosphate and/or borate monolayers.

Besides the colour characteristics, the wettability of the samples was also measured, and the statistically treated data are shown in Table 2.

Table 2. *Statistically treated data regarding the colours and wettability of CeCC/AAO layers subjected to additional sealing by borate and phosphate solutions*

Sample set	Value type	*L**	*a**	*b**	θ / °
Ref	Maximal value	85.55	-1.28	58.28	93.74
	Minimal value	83.08	-3.11	54.56	48.13
	Final result	84.52 ± 1.47	-2.08 ± 1.09	55.84 ± 2.26	63.45 ± 26.47
BB	Maximal value	86.97	-2.78	62.46	23.27
	Minimal value	84.13	-5.26	57.56	12.20
	Final result	85.79 ± 2.05	-3.84 ± 1.67	59.99 ± 3.09	19.13 ± 6.05
PB	Maximal value	86.72	-3.53	60.46	22.31
	Minimal value	84.55	-5.35	56.63	7.380
	Final result	85.40 ± 1.37	-4.62 ± 1.43	58.66 ± 2.12	12.61 ± 9.45
MB	Maximal value	87.30	-4.12	59.07	21.07
	Minimal value	84.71	-4.79	54.45	15.04
	Final result	86.01 ± 2.34	-4.53 ± 0.51	57.24 ± 3.13	18.71 ± 4.69

The treatments with phosphate/borate solutions did not result in notable changes in colour characteristics. A slight brightening of the colour, from $L^* \approx 85$ for the references to $L^* \approx 86$ for the samples treated in the mixed solution, was observed. This brightening was accompanied by a minor increase in the greenish hue, from $a^* \approx -2$ to $a^* \approx -4.5$, and a slight saturation of the yellow tonality, from $b^* \approx 55$ to $b^* \approx 60$.

Regarding contact angle, the samples changed from relatively to definitely hydrophilic after boiling in the respective buffer solutions. This effect on contact angle values is likely due to hydration during the final sealing in the buffer solutions. These initial surface characterizations were followed by topological observations of the reference and treated specimen couples using optical metallographic microscopy and scanning electron microscopy. The respective OMM and SEM images of the investigated samples are shown in Figures 3 and 4.

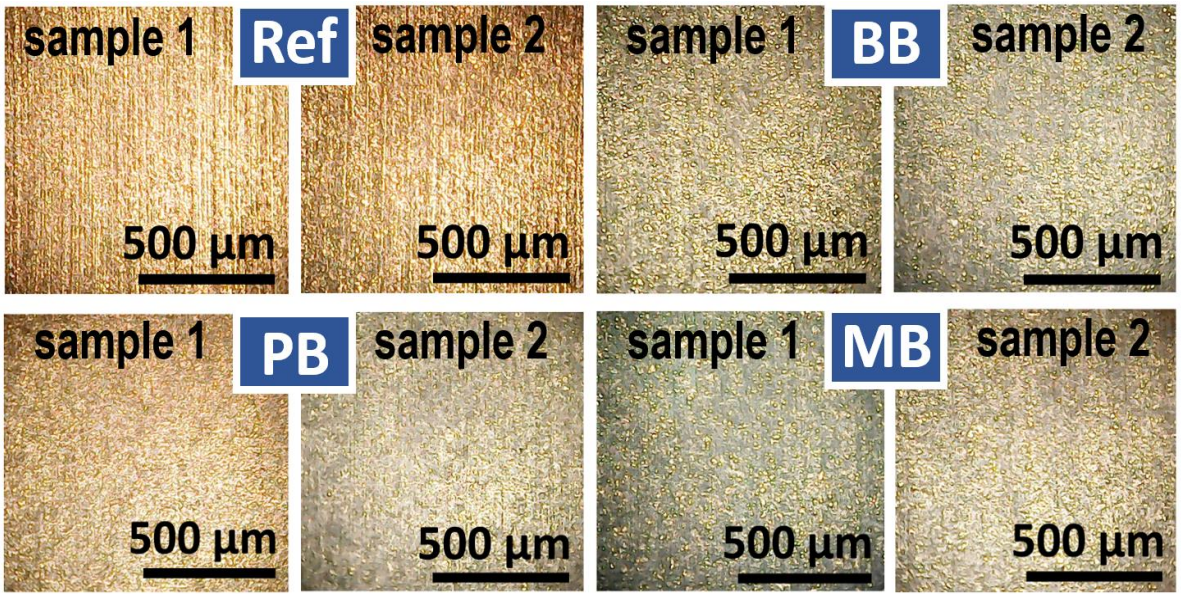

Figure 3. *OMM images of reference (Ref) and samples treated in phosphate (PB), borate (BB) and mixed (MB) buffer solutions*

The images reveal that specimens treated in borate and phosphate baths appear slightly paler than the reference specimens, although no visible alterations in topology are observable. These effects can be attributed to the inherent white colour of cerium phosphates [113-115] and borates [116,117], as well as the thin borate/phosphate monolayers expected based on described mechanisms [106,107].

SEM images, despite their higher resolution, confirm the OMM observations. All coatings, including the reference ones, appeared cracked. Therefore, the final sealing of the CeCC/AAO coating primers is necessary, as proposed in various studies [72,89-93] and supported by this research.

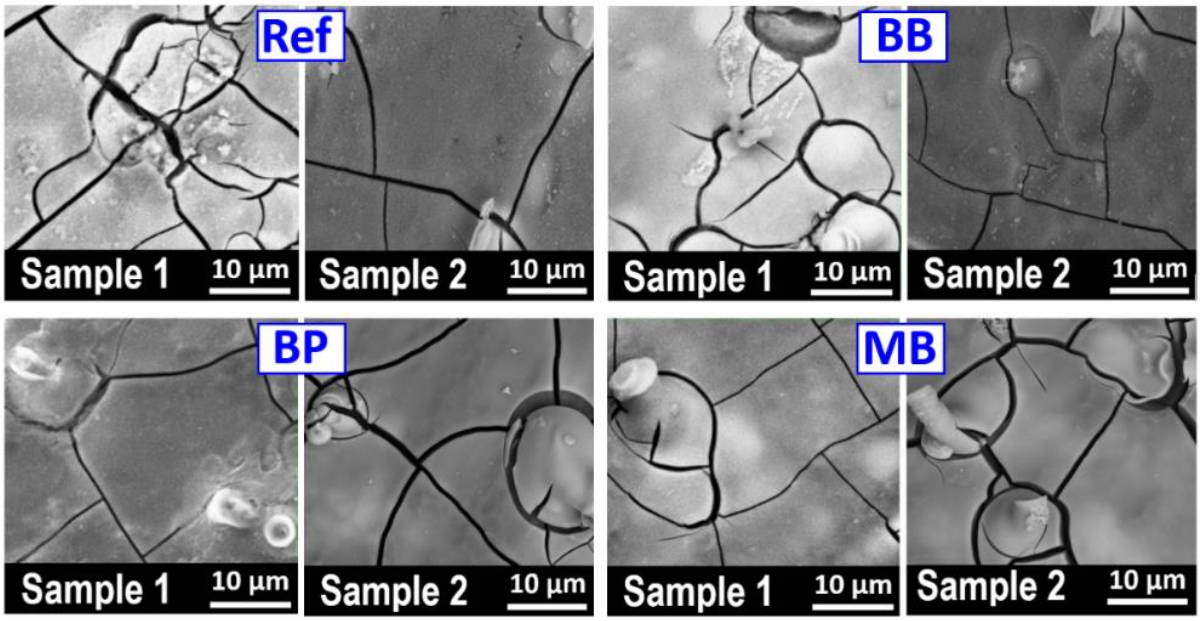

Figure 4. *SEM images of reference (Ref) and samples treated in phosphate (PB), borate (BB) and mixed (MB) buffer solutions*

In summary, the surfaces observed using both microscopy methods did not show significant differences. Boiling in the buffer solutions did not result in remarkable changes to the CeCC/AAO

layer morphologies. However, all treated specimens appeared paler, likely due to the formation of white phosphate and/or borate monolayers.

The elemental contents calculated from the XPS spectra, acquired from the phosphate/borate sealed CeCC/AAO layers, as well as the reference ones, are summarized in Table 3. This approach has enabled the definition of the impact of the final sealing procedure on the superficial primer coating compositions.

Table 3. *Data for the chemical compositions of the investigated specimens acquired through systematic XPS analyses*

Sample	Content, at.%						
	O	Al	Ce	P	B	Na	K
REF 1	75.0	7.1	17.9	0.0	0.0	0.0	0.0
REF 2	74.7	8.0	17.3	0.0	0.0	0.0	0.0
BB 1	60.0	11.2	2.6	0.0	21.7	4.2	0.0
BB 2	58.4	14.4	1.0	0.0	22.9	3.4	0.0
PB 1	61.6	2.0	0.8	16.5	0.0	18.1	1.0
PB 2	61.4	0.5	1.4	16.4	0.0	19.0	1.3
MB 1	61.2	1.1	4.3	16.5	6.5	7.9	2.5
MB 2	61.4	1.2	3.5	16.7	7.9	7.2	2.1

The data in Table 3 reveal that the reference CeCC/AAO layer covers the alloy substrate completely because the Al-concentration is nearly 7-8 at.%. The subsequent treatments in phosphate (PB) and mixed (MB) buffer resulted in a further decrement of the Al-content, down to approximately 2 at.%. In contrast, the borate buffer treatment results in a rise of the Al content up to about 11 to 14 at.%. The Al 2p core photoelectron spectra of all the sample sets are shown in Figure 5.

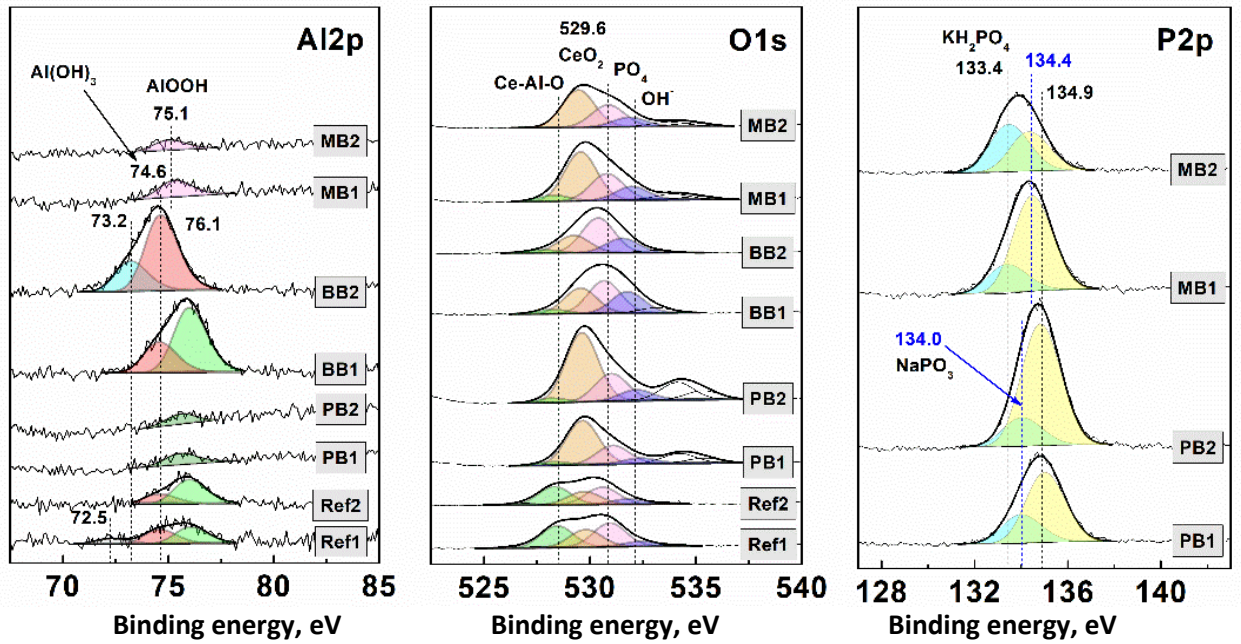

Figure 5. *Deconvolutions of XPS core photoelectron spectra of Al 2p, O 1s and P 2p. The separate peaks are with the following colours: Al2p: Al-metal - gray; $CeAlO_3$ - blue; $Al(OH)_3$ - red:, AlOOH - magenta and green; O1s: Ce-Al-O - green; Me-O - orange; PO_4^{3-} and/or BO_3^{3-}-groups - pink; OH^-/H_2O - purple; P2p: PO_4^{3-} - blue; PO_3^{3-} - green; PO_3^{3-} and BO_3^{3-} - yellow; P_2O_5 - orange*

The XPS spectra of the reference CeCC/AAO layers are split in couples of peaks positioned at 74.6 and 76.1 eV, respectively. The former peak could be attributed to the occurrence of $AlPO_4$ [118], whereas the latter is related to the presence of AlO(OH) [119]. This energy level slightly exceeds (by

0.9 eV) the characteristic one for AlO(OH), which equals 75.2 eV. This fact can be explained by the higher concentration of hydroxyl groups coordinated around the aluminium cation, which predetermines higher bonding energy, which must be overcome for the expulsion of the 2p-electrons from the electron shell of the Al-ion. The Al 2p spectrum of the Ref 1 sample has an additional low-intensity peak positioned at 72.5 eV due to metallic Al traces [116].

The Al2p spectra of the phosphate-treated samples are composed of a unique, low-intensity peak situated at 75.4 eV, which again is attributed to the presence of the AlO(OH) phase. The respective photoelectron peaks of the borate-treated specimens are more intensive and can be split into lower and higher energy ones. The former one is positioned at 74.6 eV for BB (Sample 1) and slightly shifted to 73.2 eV for BB (Sample 2), respectively. In both cases, the lower energy peak approximates the characteristic one for Al_2O_3, which, according to Latsunskyi *et al.* [120], should occur at 74.1 eV, possibly as a result of the occurrence of $Al(OH)_3$ since its typical value is 75.4 eV [121]. Thus, the shifting towards 74.6 eV could be due to $AlBO_3$ traces, whereas the opposite displacement to 73.2 eV corresponds to the characteristic one for $CeAlO_3$ [122].

The higher energy peaks are also slightly shifted to 76.1 eV for BB (Sample 1) and to 74.6 eV for BB (Sample 2), corresponding to $Al(OH)_3$ and AlO(OH), respectively.

Both mixed buffer-treated samples (MB) have only one low-intensity Al 2p peak, positioned at 75.1 eV, related to the occurrence of the AlO(OH) phase. The Al 2p spectra are particularly interesting for the CeCC/AAO layers since they show interruptions of the conversion coating. In other words, these spectra are a response of the AAO layer surface under the cracks of the CeCC layer. Thus, it could be noticed that the phosphate-containing solutions (*i.e.,* PB and MB) result in the occurrence of only the AlO(OH) phase. The samples in these groups possess rather similar corrosion protective performance. On the other hand, the borate solution treatment leads to the simultaneous occurrence of $CeAlO_3$, $Al(OH)_3$, and AlO(OH). Especially in the case of BB (Sample 2), the $CeAlO_3$ phase composes about 1/3 of the registered Al content.

The O1s photoelectron spectra are rather intensive due to the oxide composition of the entire CeCC/AAO conjunction and the presence of hydroxides and crystal hydrate water. All the investigated samples, regardless of which group they belong to, have four peaks at 528.5, 529.6, 530.9 and 532.1 eV. These peaks reveal oxygen included in both Ce-Al-O and Me-O bonds [123], as well as $(PO_4)^{3-}$, $(BO_3)^{3-}$ [124], and OH^- moieties [125]. The O1s spectra analysis reveals higher OH^- moieties content in the case of BB treatment.

The XPS analysis continued with the occurrence of phosphor as a result of the final CeCC/AAO layer sealing. The respective P2p core photoelectron spectra of the phosphate and mixed buffer-treated samples are shown in Figure 5. The photoelectron patterns of the phosphate buffer (PB) treated specimens have peaks positioned at 134.0 and 134.9 eV, corresponding to the occurrence of $(PO_4)^{3-}$ ions [126] and P_2O_5 [127], respectively. The presence of these phosphorus species is evidence for the participation of the phosphate ions in oxidation/reduction processes.

Couples of peaks are also observable for the mixed buffer-treated (MB) samples. The former peak, staying at 133.4 eV, can be attributed to the occurrence of orthophosphate $(PO_4)^{3-}$ ions. The latter one, situated at 134.4 eV, reveals $(PO_3)^{3-}$ moieties as was already commented. Shifting of the bonding energies by 0.4 eV towards higher values is probably a result of coordinated borate ligands surrounding the metallic ions.

The Ce3d photoelectron patterns were also analysed. These patterns are composed of two distinguishable peaks combined with four satellites, labelled “S” in Figure 6. The first peak is positioned at 882.3 eV, corresponding to $Ce3d_{5/2}$, while the second one is at 900.7 eV, corresponding

to $Ce3d_{3/2}$. The spin-orbital splitting between the peaks, characteristic of CeO_2, is 18.4 eV. The satellite at 916.7 eV is characteristic of Ce^{4+} ions, allowing for the calculation of its percentage of the total Ce content. The calculations reveal that the entire cerium content consists of Ce(IV) species.

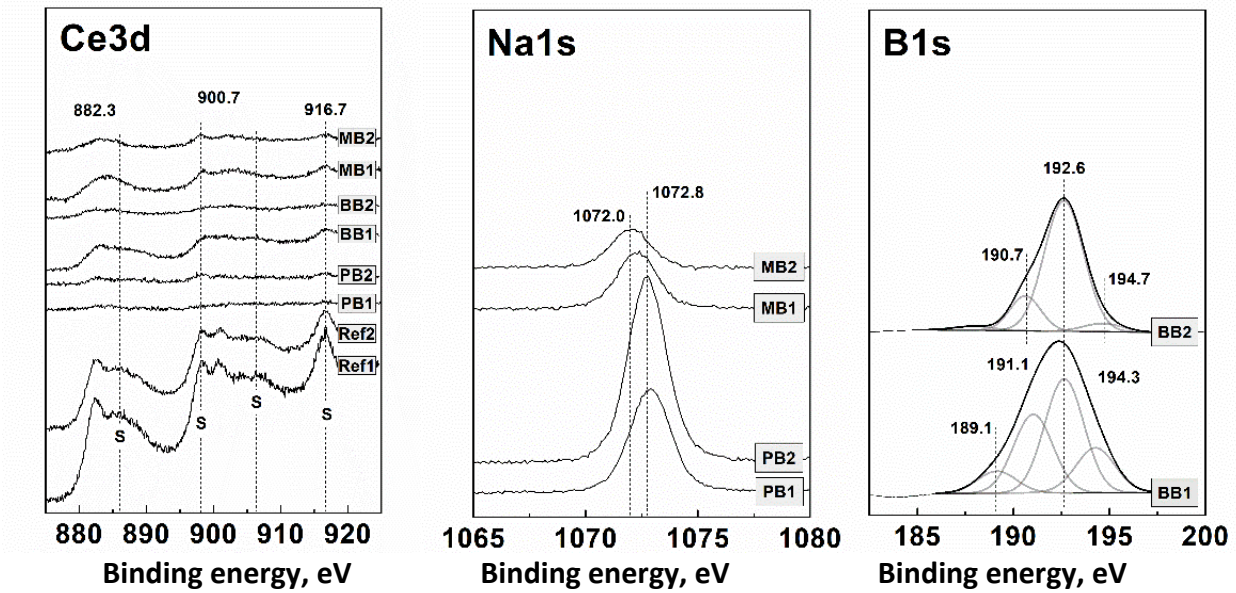

Figure 6. *Ce3d, Na1s and B1s photoelectron patterns acquired from the respective specimens*

The B1s spectra overlap with the P 2s ones. Therefore, only the B1s spectra of the borate buffer-treated samples, which lack phosphorus, were analysed. For both samples, the peaks are at a bonding energy of 192.6 eV, typical for borate ions.

The XPS spectra of the investigated coating primers exhibit well-defined repeatability, indicating the consistent application of surface treatment procedures. Additionally, the treated coating primers exhibit distinct occurrences of $(PO_3)^{3-}$, $(PO_4)^{3-}$, and P_2O_5 moieties, which are known for their low solubility [93,128]. The borate-treated coating primers have elevated aluminium contents, suggesting a partially detrimental effect of the borate solution due to the presence of HCl, which is necessary for its preparation. However, the $(B_2O_7)^{2-}$ ions form a barrier layer composed of Al_5BO_9 and/or $Al_{18}B_4O_{33}$ phases, as proposed by Luhrs *et al.* [129].

In summary, the presence of $CeAlO_3$, as indicated by the XPS spectra analysis, is the reason for the reliable and efficient corrosion protection provided by the proposed coating primers, as observed during the corrosion test results, commented below.

After 24 hours of exposure to a 3.5 % NaCl solution, 6 specimens from each set underwent electrochemical measurements. The averaged EIS data are summarized in Figure 7. The Nyquist plots reveal that despite its lower stability, BB results in notable sealing. The $\log|Z|$ - f curve is positioned above all others. At f = 0.01 Hz, the total impedance of the borate buffer-treated samples reaches $|Z|^{BB}_{av}$ = 1.8762 MΩ cm^2. This value is almost an entire order of magnitude superior to that of the reference samples $|Z|^{Ref}_{av}$ = 0.4983 MΩ cm^2. The $\log|Z|$ - f curves of the remaining specimens, treated in phosphate buffer and the mixed system, occupy intermediate positions, still above those of the reference samples. Consequently, notable sealing occurs as a result of the applied final CeCC layer treatment procedures. In brief, the ordering of the $\log|Z|$-f curves at 0.01 Hz in the respective Bode plots confirms the inferences drawn from the analysis of the Nyquist plots. The curves of the BB-treated coatings occupy the highest position. Finally, the curves of the MB-treated coatings are below those of the BB and PB-treated ones, owing to their lower barrier ability.

The *Z*''-*Z*' arcs of the BB-treated samples are the largest among the investigated sample sets. These are followed by the PB-treated ones. The mixed system shows a weaker effect on the barrier ability of the CeCC/AAO combined coating primer, as the *Z*''- *Z*'-arcs of the MB-treated specimens are closer to those of the references compared to the rest of the curves.

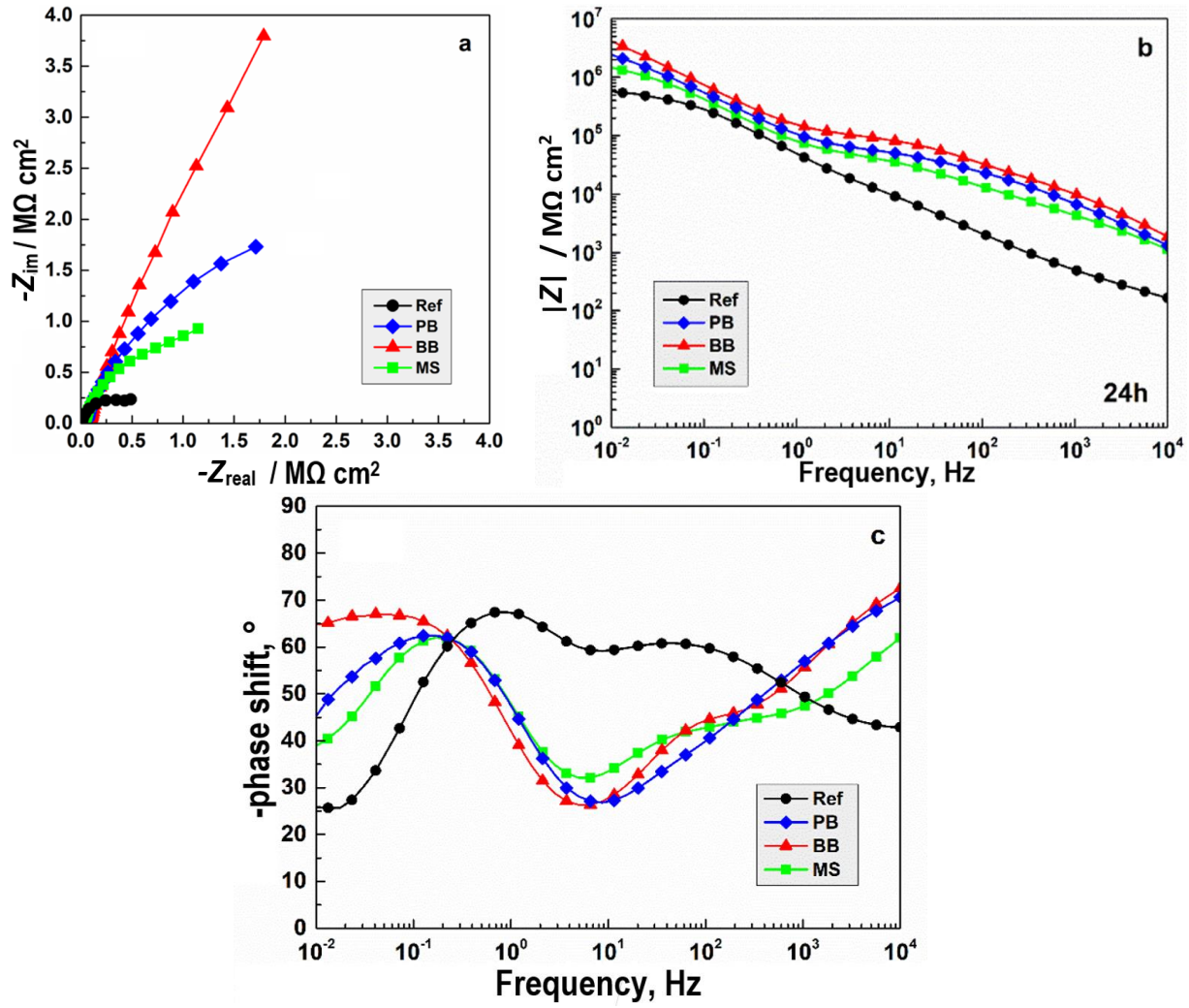

***Figure 7**. Nyquist (a) and Bode (b, c) plots acquired after 24 hours of exposure to MCM from CeCC/AAO layers subjected to sealing in boiling buffer solutions*

The EIS spectra shown in Figure 7 were further analysed *via* data fitting to suitable model equivalent circuits (MECs), as depicted in Figure 8. Following the concepts outlined in [105], these MECs represent the charge transfer across homogeneous media through ohmic resistance elements, while the charge transfer across interfaces is represented by either pure capacitance or by constant phase elements due to the related charge accumulation phenomena.

The MECs shown in Figure 8 are composed considering the main concepts of González-Castaño *et al.* [130] and González-Rovira *et al.* [131]. In both schemes, C_{layer} is attributed to the intact, nonconductive layer areas. This element is connected in parallel with time constants, resulting from the penetration of the electrolyte (R_{layer}) across the layer defects and the electrochemical corrosion reactions (R_{ct}) after overcoming the double layer (CPE_{dl}). Hence, C_{layer} appeared suitable during the EIS data fitting, although the phase shift-frequency diagrams did not reach 90°. The reason is that the capacitance of the intact areas of the CeCC/AAO layers is connected in parallel to the elements (*i.e.,* R_{layer}, CPE_{dl}, R_{ct} and CPE_{diff}) attributed to the defects of the layers, resulting in phase shift values below 90 °.

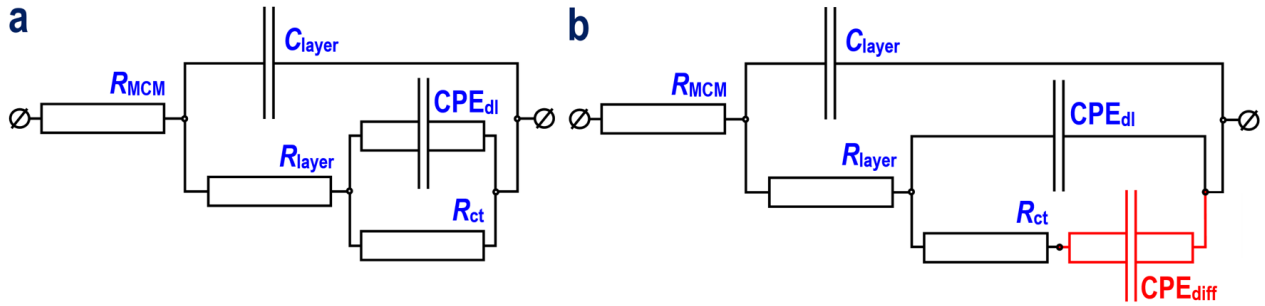

Figure 8. *MECs used for data fitting of the spectra of the reference (a) and sealed CeCC/AAO layer (b). R_{MCM} - resistance of the model corrosive medium; R_{layer} - resistance of the electrolyte penetrated across the CeCC/AAO layer defects; R_{ct} - charge transfer resistance; R_{diff} - resistance arising from the diffusion of the corrosive species across the coating primer defects; C_{layer} - capacitance originated from the insulating properties of the CeCC/AAO layer; CPE_{dl} and CPE_{diff} - incomplete capacitances of the electric double layer and the diffusion processes inside the layer defects*

Indeed, a multitude of cracks is notable in the SEM images of Figure 4. When these defects are narrow enough, re-passivation occurs, as outlined in [132,133]. Otherwise, these defects continue as crevices. Their occurrence results in the appearance of CPE_{dl} and R_{diff} time constants. They demonstrate stagnant corrosion, hindered by capillary diffusion across the corrosion products with "Keggin"-type $(Al_{13}O_4(OH)_{24}(H2O)_{12})^{7+}$ and $(AlO_4Al_{12}(OH)_{24}(H2O)_{12})^{7+}$ aluminum polyhydroxychloride structures, like established in [134,135]. The fitting of the EIS spectra in Figure 7 was performed using the MEC illustrated in Figure 8. All the acquired data are summarized in Table 4.

Table 4. *Results of the data fitting of the MEC in Figure 8 to EIS spectra shown in Figure 7*

MEC component (24 h)	Sample sets			
	Ref samples	BB samples	PB samples	MB samples
R_{MCM} / Ω cm^2	225.4 ± 24.5	206.6 ± 20.8	194.0 ± 18.8	163.5 ± 28.1
C_{layer} / nF cm^{-2}	51.3 ± 4.5	8.5 ± 0.2	10.5 ± 0.3	13.0 ± 0.5
R_{layer} / kΩ cm^2	2.2 ± 0.2	7.1 ± 0.6	2.2 ± 0.3	2.2 ± 0.1
CPE_{edl} / 10^{-7} s^n Ω^{-1} cm^{-2}	36.5 ± 1.8	5.7 ± 0.4	10.1 ± 2.3	17.9 ± 0.6
n	0.66 ± 0.01	0.59 ± 0.01	0.53 ± 0.01	0.57 ± 0.01
R_{ct} / kΩ cm^2	988.0 ± 18.6	133.2 ± 4.5	81.6 ± 1.3	85.5 ± 3.0
CPE_{diff} / 10^{-7} s^n Ω^{-1} cm^{-2}	-	14.9 ± 0.5	16.7 ± 1.27	16.5 ± 0.7
n	-	0.89 ± 0.01	0.91 ± 0.01	0.99 ± 0.01
R_{diff} / MΩ cm^2	-	65.1 ± 3.1	8.4 ± 0.4	3.4 ± 0.2

The data in the table indicate that the reference samples did not require the addition of diffusion elements (CPE_{diff} and R_{diff}) to fit their spectra, unlike the additionally treated ones. This fact suggests that the CeCC/AAO layer maintained its integrity after 24 hours of exposure. However, all the buffer-treated specimens required the addition of diffusion elements, indicating corrosion occurrence combined with diffusion limitations.

Consequently, boiling resulted in coating cracking due to thermal tensions caused by the relatively high temperature. Nevertheless, the R_{diff} element exhibited rather high values, falling within the range of R_{ct} of the reference samples. Moreover, in the case of borate buffer (BB) treated samples, the sum of R_{ct} and R_{diff} was two orders of magnitude higher than the R_{ct} value for the reference specimens. This fact accounts for the superior barrier ability of these samples, as mentioned earlier. The R_{ct} and R_{diff} values in the cases of PB and MB are inferior to those of the borate-treated samples, further emphasizing the superior barrier ability of the BB-treated ones.

This inference is supported by the highest R_{ct} and R_{layer} values obtained from the borate buffer-treated samples compared to those of the other specimen sets. Additionally, the highest corrosion

protection of the borate buffer-treated samples is evident from the EIS spectra shapes in Figure 7, as indicated by the highest position of the log|*Z*|-*f* curve at 0.01 Hz in the Nyquist plot (Figure 7a), corresponding to 4.198 MΩ cm^2, and the largest arc of these specimens in the respective Bode plots (Figure 7b and c).

Following every EIS spectrum recording, potentiodynamic curve acquisition was performed. The averaged PDS curves are summarized in Figure 9. The PDS curves of the sealed specimens are positioned below the reference ones, indicating lower current densities. Consequently, the respective sealings should have a beneficial effect on the barrier properties of the treated CeCC/AAO layers. Furthermore, the PDS curve with the lowest current densities is registered for the BB-treated specimens.

All the curves shown in Figure 9 exhibit passivation regions combined with local corrosion features. In the cases of buffer solution treatments, these regions possess weak slopes, suggesting incomplete passivation. The occurrence of local corrosion is noticeable by the sharp bending of the anodic branches, indicating pitting corrosion. However, the difference among the sample types is evident from the curve positions. The curves of reference samples are positioned at the highest current densities and the most negative potential values, whereas the BB ones are situated at the lowest current densities and the noblest potentials. The final treatments in phosphate and mixed solutions result in intermediate positions of the PDS curves, relatively closer to the curves of the reference samples.

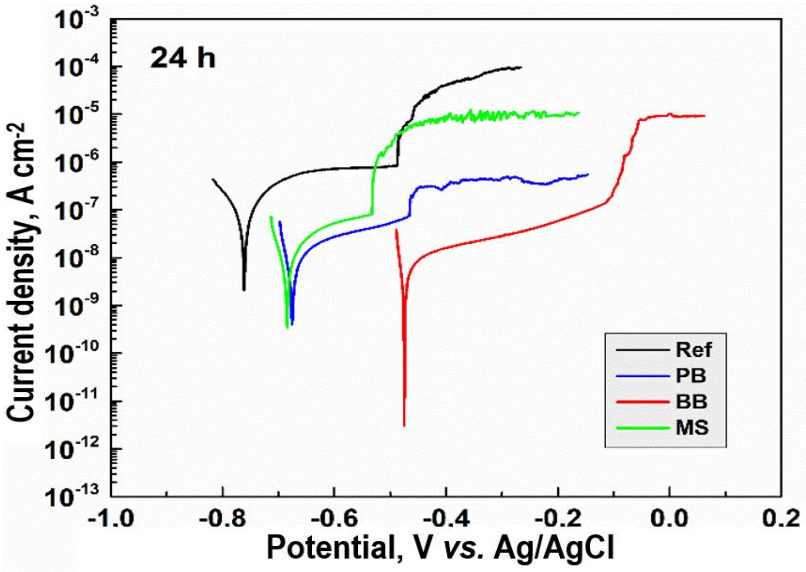

Figure 9. *PDS curves obtained from the reference and sealed CeCC/AAO layers*

In summary, an ambiguous effect is to be expected from the final sealing procedure. On one hand, the buffer solutions should result in the formation of thin sealing layers, leading to an increment of the resistance values. On the other hand, boiling should cause CeCC/AAO layer cracking. In the present case, the borate buffer (BB) reveals the most notable beneficial effect compared to the rest (PB and MB). The borate and phosphate buffers (MB) mixture reveals the weakest impact on the coating primer performance. The inferior behaviour of the phosphate-treated samples compared to the borate-treated ones can be explained by considering the observed alkalization (mentioned at the beginning of the "Results and Discussion" section) of its solution, which affects the amphoteric AAO layer under the cracks of the CeCC film, as noticeable in the SEM images (Figure 4).

The curves shown in Figure 9 were further subjected to Tafel slope analysis and the results are shown in Table 5.

Table 5. *Results of the Tafel slope analysis of the PDS curves acquired after 24 hours of exposure to 3.5 % NaCl model corrosive medium*

Sample type	OCP, mV	E_{corr} / mV	i_{corr} / nA cm^{-2}	R_p / MΩ cm^2	E_{pit} / mV	i_{pit} / nA cm^{-2}
Ref	-767 ± 13	-761 ± 15	(2.1 ± 0.1) 10^3	0.17 ± 0.02	-488 ± 19	(8.4 ± 0.7) 10^3
BB	-479 ± 17	-475 ± 16	2.75 ± 0.16	1.63 ± 0.28	-114 ± 10	71.12 ± 6.72
PB	-687 ± 12	-676 ± 18	7.41 ± 0.18	1.41 ± 0.27	-466 ± 18	74.01 ± 2.04
MB	-611 ± 18	-615 ± 16	3.74 ± 0.15	1.40 ± 0.22	-473 ± 27	52.83 ± 6.94

The results in Table 5 confirm the inferences drawn from the analysis of Figure 9, substantiating them with numerical values of the electrochemical measures. Notably, a significant difference is observed among the values of the open circuit potential (OCP) and the corrosion potential (E_{corr}), as a result of the final treatments of the CeCC/AAO layers. The data in the table show a rather large range of nearly 300 mV between the reference samples (Ref) and the borate solution-treated (BB) ones. The former tends to about -770 mV, whereas the latter approaches -480 mV. The intermediate OCP and E_{corr} values are possessed by the PB and MB buffer solution-treated specimens, with about -670 and -620 mV, respectively.

Further analysis of the data in Table 5 reveals that the most negative E_{corr} values of the reference samples are associated with three orders of magnitude higher corrosion current density (i_{corr}). Consequently, the final CeCC/AAO layers treatment results in an obvious enhancement of the barrier ability of the CeCC/AAO layers, suppressing the i_{corr} down to about 5 nA cm^{-2}. Once again, the lowest corrosion current density belongs to the BB-treated specimens. A similar difference is also noticeable in the polarization resistance (R_p) values. Hence, the R_p of the additionally treated specimens is more than an order of magnitude higher than those of the references. Besides, the BB-treated CeCC/AAO layers possess the highest R_p values.

Additional analysis was performed on the anodic branches of the PDS curves, providing supplemental data regarding the pitting corrosion parameters, namely pitting potential (E_{pit}) and current density (i_{pit}). The former measure provides the determination of the strength against pitting nucleation (SAPN = E_{corr} - E_{pit} [105]), whereas the latter enables the calculation of the pitting nucleation resistance (R_{pit}). The SAPN values for the references and the borate buffer-treated ones are approximately $SAPN_{Ref}$ ≈ 273 mV and $SAPN_{BB}$ ≈ 361 mV, respectively. Since a higher SAPN value indicates a larger passivation region, the BB-treated samples also excel in the reference ones in this parameter. The SAPN of the PB and MB samples exhibit even lower values.

The ratio between i_{pit} and E_{pit} allows the estimation of the R_{pit} values for the respective sample sets. Thus, the BB specimens have R_{pit}^{BB} ≈ 1.603 MΩ cm^2, whereas R_{pit}^{Ref} ≈ 0.581 MΩ cm^2. The rest of the treated sample sets have shown R_{pit}^{PB} ≈ 6.296 MΩ cm^2 and R_{pit}^{MB} ≈ 8.953 MΩ cm^2, respectively. These values are slightly higher than those of the borate buffer-treated specimens. Nevertheless, the final treatment in all cases results in rather higher R_{pit} values compared to those of the references.

In summary, comparing the results of both electroanalytical methods (Tables 4 and 5) enables the ordering of the effects of each buffer on the barrier properties of the CeCC/AAO layers. Thus, in accordance with both electroanalytical methods, the highest protective ability belongs to the BB set, followed by PB and finally MB. The same ordering from the best to the worst barrier properties can be seen in Figures 7 and 9, summarized as BB > PB > MB > Ref. The analyses above reveal that this order is confirmed by both electrochemical methods employed. Consequently, in simple words, the treatment by borate buffer possesses a better sealing effect on the CeCC/AAO layer than that by phosphate solution and no synergistic effect between these solutions appeared, although the expectations.

Conclusions

This study is focused on the sealing of CeCC/AAO layers using Lourier buffers with relatively neutral pH. It presents the results of systematic research conducted on four sample sets, each comprising eight CeCC/AAO combined coating primers deposited on AA2024-T3 alloy. Three sets underwent additional sealing in borate (BB), phosphate (PB), and mixed (MB) buffers. Two samples from each set underwent comparative analyses of their properties, including colour and wettability, as well as topological analyses using optical and electron microscopy methods and detailed chemical composition determination via X-ray photoelectron spectroscopy (XPS).

The remaining six samples from each set were subjected to electrochemical tests using electrochemical impedance spectroscopy (EIS) and potentiodynamic scanning (PDS) after 24 hours of exposure to 3.5 % NaCl model corrosive medium.

The results indicate that the applied sealing procedures do not affect the topology of the CeCC/AAO layer but alter the surface chemical composition and resulting surface properties. While the micrographs show identical topologies, the sealed specimens exhibit increased hydrophilicity and paler coloration. These alterations in surface properties are attributed to changes in chemical composition detected by XPS analysis, which reveals the presence of $(PO_4)^{3-}$, $(BO_3)^{3-}$, $(B_2O_7)^{2-}$ and OH^- moieties, likely forming thin monolayers based on literature analysis.

Corrosion tests demonstrate that among the tested buffer solutions, the borate solutions have a superior effect despite their Cl^- ion content. The beneficial effect of the phosphate solutions was comparatively weaker. Additionally, mixing borate and phosphate buffers did not result in synergistic effects as initially expected.

Sealing with phosphate and/or borate buffers enables the formation of sealing layers, but it is important to perform these procedures at lower temperatures. Otherwise, the solutions may change their composition due to precipitation, resulting in pH alterations that affect the amphoteric AAO layer beneath the cracks of the CeCC film.

Acknowledgements*: The authors express their gratitude for the financial support provided by the Bulgarian National Scientific Fund under Contract No. КП-06-Н79/1(2023) for the project "Protective and functional layers on aluminum and its alloys". Research equipment of the distributed researchinfrastructure INFRAMAT (part of the Bulgarian National roadmap for research infrastructure) supported by the Bulgarian Ministry of Education and Science was also used in this investigation.*

References

[1] E. Georgantzia, M. Gkantou, G. S. Kamaris, Aluminium alloys as structural material: A review of research, *Engineering Structures* **227** (2021) 111372. http://doi.org/10.1016/j.engstruct.2020.111372

[2] N. Li, X. Yan, X. Liu, L. Han, W. Zhang, Mechanical Properties Evolution of the 7B04-T74 Aluminum Alloy in the Marine Atmosphere, *Metals* **12(12)** (2022) 2173. https://doi.org/10.3390/met12122173

[3] M. Nisar, M. S. Charoo, A Comparative Analysis of Corrosion Performance of Piston Alloy and Its Composite in Marine, Mining and Basic Environments, *Journal of Bio- and Tribo-Corrosion* **8** (2022) 42. https://doi.org/10.1007/s40735-022-00645-5

[4] L. Luo, B. Wang, J. Zhou, J. Liu, X. Wang, Effect of Cyclic Stress on Corrosion Behavior of 7A09 Aluminum Alloy in Tropical Coastal Atmosphere, *International Journal of Electrochemical Science* **17** (2022) 221215. http://doi.org/10.20964/2022.12.03

[5] H. S. Lai, Xiaowei Jiang, H. Li, H. Cui, Z. Zhao, H. Guo, L. Li, Investigation of 7075 Aluminum Alloy Corrosion in Marine Environment, *International Journal of Electrochemical Science* **17** (2022) 220559. http://doi.org/10.20964/2022.05.56

[6] Y. Wan, L. Li, Y. Jin, Y. Li, X. Zhu, Pitting corrosion behavior and mechanism of 5083 aluminum alloy based on dry-wet cycle exposure, *Materials and Corrosion* **74(4)** (2023) 608-621. https://doi.org/10.1002/maco.202213546

[7] L. Shi, L. Xiang, J. Tao, Q. Chen, J. Liu, Y. Zhong, Actual Marine Atmospheric Pre-Corrosion Fatigue Performance of 7075-T73 Aluminum Alloy, *Metals* **12(5)** (2022) 874. https://doi.org/10.3390/met12050874

[8] A. Gnanavelbabu, X. J. Amul, K. T. S. Surendran, Investigation on the tribocorrosion and electrochemical corrosion behaviour of AA2014/Al_2O_3 nanocomposites fabricated through ultrasonication coupled stir-squeeze casting method, *Journal of Applied Electrochemistry* **52(4)** (2022) 765-791. http://doi.org/10.1007/s10800-022-01666-1

[9] Y. Zhu, H. Liu, D. Zhang, J. Wang, F. Yan, Effect of polarization potentials on tribocorrosion behavior of Monel 400 alloy in seawater environment, *Tribology International* **168** (2022) 107445. http://doi.org/10.1016/j.triboint.2022.107445

[10] J. G. Boomadevi, J. R. Xavier, Effect of indole functionalized nano-alumina on the corrosion protection performance of epoxy coatings in marine environment, *Journal of Macromolecular Science* **A-57(10)** (2020) 691-702. http://doi.org/10.1080/10601325.2020.1761831

[11] K. Rajitha, K. N. S. Mohana, Synthesis of graphene oxide-based nanofillers and their influence on the anticorrosion performance of epoxy coating in saline medium, *Diamond and Related Materials* **108** (2020) 107974. http://doi.org/10.1016/j.diamond.2020.107974

[12] V. S. Egorkin, I. M. Medvedev, S. L. Sinebryukhov, I. E. Vyaliy, A. S. Gnedenkov, K. V. Nadaraya, N. V. Izotov, D. V. Mashtalyar, S. V. Gnedenkov, Atmospheric and marine corrosion of PEO and composite coatings obtained on Al-Cu-Mg aluminum alloy, *Materials* **13(12)** (2020) 2739. http://doi.org/10.3390/ma13122739

[13] M. Acila, H. Bensabra, M. Santamaria, Study of the influence of dithizone as an eco-friendly corrosion inhibitor on the corrosion behaviour of AA7075 aluminium alloy in neutral chloride solution, *Metallurgical Research and Technology* **118(2)** (2021) 2021002. http://doi.org/10.1051/metal/2021002

[14] D. Marunkić, J. Pejić, B. Jegdić, S. Linić, J. Perišić, B. Radojković, A. Marinković, Inhibitory Effect of Cerium Salts of Lower Carboxylic Acids on Al-Zn-Mg-Cu Alloy in NaCl Solution, *Journal of The Electrochemical Society* **168(8)** (2021) 081501. http://doi.org/10.1149/1945-7111/ac1895

[15] J. Pejić, B. Radojković, D. Marunkić, B. Jegdić, S. Stevanović, M. Milošević, J. Bajat, Inhibitory effect of cysteine and lanthanides on AA7075-T6 in neutral NaCl solution, *Materials and Corrosion* **73(11)** (2022) 1800-1812. http://doi.org/10.1002/maco.202213330

[16] S. Bhaskara, S. P. Fakrudeen, T. Desalegn, H. C. A. Murthy, V. Bheemaraju, Evaluation of Corrosion Inhibition Efficiency of Aluminum Alloy 2024 by Diaminostilbene and Azobenzene Schiff Bases in 1 M Hydrochloric Acid, *International Journal of Corrosion* **2021** (2021) 5869915. http://doi.org/10.1155/2021/5869915

[17] Ch. Girginov, S. Kozhukharov, M. Milanes, M. Machkova, Impact of the anodizing duration on the surface morphology and performance of A2024-T3 in a model corrosive medium, *Materials Chemistry and Physics* **198** (2017) 137-144. https://doi.org/10.1016/j.matchemphys.2017.05.049

[18] T. Hashimoto, M. Curioni, X. Zhou, J. Mancuso, P. Skeldon, G. E. Thompson, Investigation of dealloying by ultra-high-resolution nanotomography, *Surface and Interface Analysis* **45(10)** (2013) 1548-1552. https://doi.org/10.1002/sia.5176

[19] M. B. B. Sultan, D. Thierry, J. M. Torrescano-Alvarez, K. Ogle, Selective dissolution during acid pickling of aluminum alloys by element-resolved electrochemistry, *Electrochimica Acta* **404** (2022) 139737. http://doi.org/10.1016/j.electacta.2021.139737

[20] E. Mysliu, K. Sletteberg Storli, E. Kjørsvik, O. Lunder, A. Erbe, Recycled Aluminium Alloys and their Models: Role and Behaviour of Alloying Elements during Alkaline Etching, *Journal of The Electrochemical Society* **170** (2023) 011503. http://doi.org/10.1149/1945-7111/acb38a

[21] M. B. B. Sultan, D.Thierry, K. Ogle, On the dissolution rates and mechanisms of Al-Mg and Al-Cu alloys during acid pickling using element-resolved electrochemistry, *Electrochimica Acta* **444** (2023) 141961. http://doi.org/10.1016/j.electacta.2023.141961

[22] A. Kosari, F. Tichelaar, P. Visser, H. Zandbergen, H. Terryn, J. M. C. Mol, Dealloying-driven local corrosion by intermetallic constituent particles and dispersoids in aerospace aluminium alloys, *Corrosion Science* **177** (2020) 108947. https://doi.org/10.1016/j.corsci.2020.108947

[23] W. Zhang, G. S Frankel, Transitions between pitting and intergranular corrosion in AA2024, *Electrochimica Acta* **48(9)** (2003) 1193-1210. https://doi.org/10.1016/S0013-4686(02)00828-9

[24] P. Rodič, I. Milošev, G. S. Frankel, Corrosion of Synthetic Intermetallic Compounds and AA7075-T6 in Dilute Harrison's Solution and Inhibition by Cerium(III) Salts, *Journal of The Electrochemical Society* **170** (2023) 031503. http://doi.org/10.1149/1945-7111/acc0a3

[25] X. Zhang, X. Zhou, T. Hashimoto, B. Liu, Localized corrosion in AA2024-T351 aluminium alloy: Transition from intergranular corrosion to crystallographic pitting, *Materials Characterization* **130** (2017) 230-236. http://doi.org/10.1016/j.matchar.2017.06.022

[26] R.M. Katona, E.K. Karasz, R.F. Schaller, A Review of the Governing Factors in Pit-to-Crack Transitions of Metallic Structures, *Corrosion* **79(1)** (2023) 72-96. https://doi.org/10.5006/4179

[27] N. D. Alexopoulos, Z. Velonaki, C. I. Stergiou, S. K. Kourkoulis, The effect of artificial ageing heat treatments on the corrosion-induced hydrogen embrittlement of 2024 (Al-Cu) aluminium alloy, *Corrosion Science* **102** (2016) 413-424. https://doi.org/10.1016/j.corsci.2015.10.034

[28] M. A. El-Hashemy, A. E. Hughes, T. Gengenbach, A. M. Glenn, I. S. Cole, Combined influence of Ce(III) and iodide ions for corrosion protection of AA 2024-T3 in acidic to neutral chloride-rich environments: Electrochemical and surface characterization studies, *Journal of Rare Earths* **41(2)** (2023) 309-320. http://doi.org/10.1016/j.jre.2022.05.014

[29] J. Wang, J. Zhao, M. Tabish, F. Shi, Q. Cheng, L. Peng, Protection of Zn-Mg-Al coated steel corrosion by cerium gluconate in 0.05 M NaCl solution, *Journal of Molecular Liquids* **3611** (2022) 119595. http://doi.org/10.1016/j.molliq.2022.119595

[30] M. A. A. Khan, O. M. Irfan, F. Djavanroodi, M. Asad, Development of Sustainable Inhibitors for Corrosion Control, *Sustainability* (Switzerland) **14** (2022) 9502. http://doi.org/10.3390/su14159502

[31] H. Wei, J. Tang, X. Chen, Y. Tang, X. Zhao, Y. Zuo, Influence of organic and inorganic cerium salts on the protective performance of epoxy coating, *Progress in Organic Coatings* **166** (2022) 106763. http://doi.org/10.1016/j.porgcoat.2022.106763

[32] R. Lopez-Sesenes, J. G. Gonzalez-Rodriguez, J. G. Vera-Dimas, R. Guardian-Tapia, L. Cisneros-Villalobos, Organic and inorganic compounds as corrosion inhibitors to reduce galvanic effect for the hybrid structure AA2024-CFPR *Journal of Electrochemical Science and Engineering* **12(2)** (2022) 343-358. http://doi.org/10.5599/jese.1126

[33] X. T. Xu, H. W. Xu, Y. Wang, X. Y. Zhang, X. J. Tan, Cerium chloride and L-arginine as effective hybrid corrosion inhibitor for 5052 aluminum alloy in 3.5% NaCl solution,

International Journal of Electrochemical Science **17** (2022) 221226. http://doi.org/10.20964/2022.12.24

[34] D. Kotnarowska, A. Zabinska, Influence of aqueous sodium chloride solutions on operational properties of epoxy coatings, *Eksploatacja i Niezawodnošć – Maintenance and Reliability* **24(4)** (2022) 629-640. http://doi.org/10.17531/ein.2022.4.4

[35] A. M. Semiletov, A. A. Kudelina, Yu. I. Kuznetsov, New prospects in the application of superhydrophobic coatings and corrosion inhibitors, *International Journal of Corrosion and Scale Inhibition* **11(3)** (2022) 1388-1400. http://doi.org/10.17675/2305-6894-2022-11-3-28

[36] L. R. B. Hari, A. Ashwin, V. R. Vaira, S. C. B. Chand, M. Vignesh, R. Padmanaban, Corrosion and tribological behaviour of Friction Stir Processed AA2024-T351 alloy, *Corrosion and Material Protection Journal – Koroze a Ochrana Materialu* **66(1)** (2022) 81-95. http://doi.org/10.2478/kom-2022-0012

[37] I. A. W. Ma, Sh. Ammar, S. S. A. Kumar, K. Ramesh, S. Ramesh, A concise review on corrosion inhibitors: types, mechanisms and electrochemical evaluation studies, *Journal of Coatings Technology and Research* **19(1)** (2022) 241-268. http://doi.org/10.1007/s11998-021-00547-0

[38] S. Zheng, F. Zhang, Y. Liu, S. Ouyang, Y. W. Ye, H. Chen, Synthesis of Ce, N co-doped carbon dots as green and effective corrosion inhibitor for copper in acid environment, *Journal of the Taiwan Institute of Chemical Engineers* **141** (2022) 104608. http://doi.org/10.1016/j.jtice.2022.104608

[39] B. Jegdić, B. Bobić, B. Radojković, J. Kovačina, D. Marunkić, Synergistic effect of $CeCl_3$ and benzotriazole on corrosion resistance of naturally aged and artificially, aged AA2024 aluminium alloy, *Transactions of Nonferrous Metals Society of China* **30(6)** (2020) 1478-1490. http://doi.org/10.1016/S1003-6326(20)65312-2

[40] T. T. Nguyen, C. Arrighi, T. T. Thai, L. Dangreau, M. F. Gonon, A. T. Trinh, M-G. Olivier, Inhibitive effect of the Ce (III) chloride and nitrate on the corrosion resistance of Zn alloyed sacrificial coatings: Effect of alloying compounds of the sacrificial layer, *Electrochimica Acta* **4521** (2023) 142296. https://doi.org/10.1016/j.electacta.2023.142296

[41] J. Panchal, D. Shah, R. Patel, S. Shah, M. Prajapati, M. Shah, Comprehensive Review and Critical Data Analysis on Corrosion and Emphasizing on Green Eco-friendly Corrosion Inhibitors for Oil and Gas Industries, *Journal of Bio- and Tribo- Corrosion* **7(3)** (2021) 107. http://doi.org/10.1007/s40735-021-00540-5

[42] M. Gobara, A. Baraka, R. Akid, M. Zorainy, Corrosion protection mechanism of Ce^{4+}/organic inhibitor for AA2024 in 3.5% NaCl, *RSC Advances* **10** (2020) 2227-2240. http://doi.org.10.1039/C9RA09552G

[43] H. Wei, B. Heidarshenas, L. Zhou, G. Hussain, Q. Li, K. K. Ostrikov, Green inhibitors for steel corrosion in acidic environment: state of art, *Materials Today Sustainability* **10** (2020) 100044. https://doi.org/10.1016/j.mtsust.2020.100044

[44] P. Rodič, M. Lekka, F. Andreatta, I. Milošev, L. Fedrizzi, The synergistic effect of cerium acetate and sodium sulphate on corrosion inhibition of AA2024-T3 at various temperatures, *Electrochimica Acta* **370** (2021) 137664. http://doi.org/10.1016/j.electacta.2020.137664

[45] P. J. Denissen, A. M Homborg, S. J. Garcia, Requirements for corrosion inhibitor release from damaged primers for stable protection: A simulation and experimental approach using cerium loaded carriers, *Surface and Coatings Technology* **430** (2022) 127966. http://doi.org/10.1016/j.surfcoat.2021.127966

[46] P. Rajendran, A. Muthuraj, N. E. Rajagounder, Review on CeO_2-Based Corrosion Coatings, *Transactions of the Indian Ceramic Society* **81(4)** (2022) 158-174. http://doi.org/10.1080/0371750X.2022.2149623

[47] S. V. Harb, M. S. Rodrigues, T. A. C. de Souza, A. Trentin, M. C. Uvida, D. J. Pochapski, S. H. Polcinelli, C. V. Santilli, P. Hammer, Smart PMMA cerium oxide anticorrosive coatings: Effect of ceria content on structure and electrochemical properties, *Progress in Organic Coatings* **161** (2021) 106548. http://doi.org/10.1016/j.porgcoat.2021.106548

[48] R. del Olmo, M. Mohedano, P. Visser, A. Rodriguez, E. Matykina, R. Arrabal, Effect of cerium (IV) on thin sulfuric acid anodizing of 2024-T3 alloy, *Journal of Materials Research and Technology* **15** (2021) 3240-3254. http://doi.org/10.1016/j.jmrt.2021.09.117

[49] V. K. S. Srikant, V. Kumar, R. S. Joshi, S. Jain, P. Kumar, A Review of Recent Research on Rare Earth Particulate Composite Materials and Structures with Their Applications, *Transactions of the Indian Institute of Metals* **74(11)** (2021) 2569-2581. http://doi.org/10.1007/s12666-021-02338-y

[50] S. Abirami, T. Bharathidasan, S. Sathiyanarayanan, C. Arunchandran, Cerium Stearate Electrodeposited Superhydrophobic Coatings for Active Corrosion Protection of Anodized AA2024-T3, *Corrosion* **77(10)** (2021) 1080-1099. http://doi.org/10.5006/3799

[51] R. del Olmo, U. Tiringer, I. Milošev, P. Visser, R. Arrabal, E. Matykina, J. M. C. Mol, Hybrid sol-gel coatings applied on anodized AA2024-T3 for active corrosion protection, *Surface and Coatings Technology* **419** (2021) 127251. http://doi.org/10.1016/j.surfcoat.2021.127251

[52] V. K. Sharma, V. Kumar, R. S. Joshi, Manufacturing of stable hydrophobic surface on rare-earth oxides aluminium hybrid composite, *Journal of Process Mechanical Engineering* **235(4)** (2021) 899-912. http://doi.org/10.1177/0954408920979105

[53] T. Zehra, M. Kaseem, Lanthanides: The Key to Durable and Sustainable Corrosion Protection, *ACS Sustainable Chemistry & Engineering* **11(18)** (2023) 6776-6800. https://doi.org/10.1021/acssuschemeng.3c00763

[54] L. Jiang, Y. Dong, Y. Yuan, X. Zhou, Y. Liu, X. Meng, Recent advances of metal-organic frameworks in corrosion protection: From synthesis to applications, *Chemical Engineering Journal* **430(3)** (2022) 132823. https://doi.org/10.1016/j.cej.2021.132823

[55] M. Motamedi, M. Ramezanzadeh, B. Ramezanzadeh, M. Mahdavian, One-pot synthesis and construction of a high performance metal-organic structured nano pigment based on nanoceria decorated cerium (III)-imidazole network (NC/CIN) for effective epoxy composite coating anti-corrosion and thermo-mechanical properties improvement, *Chemical Engineering Journal* **382** (2020) 122820. https://doi.org/10.1016/j.cej.2019.122820

[56] I. Milošev, B. Kapun, P. Rodič, The Relation Between the Microstructure of Aluminum Alloy 7075-T6 and the Type of Cerium Salt in the Formation of the Cerium Conversion Layer, *Journal of The Electrochemical Society* **169** (2022) 091501. https://doi.org/10.1149/1945-7111/ac8d35

[57] A. Petica, A. C. Manea, G. Mihai, I. Nicola, V. Ceara, L. Anicai, Cerium-based conversion films developed on LiAl-layered double hydroxide coatings for corrosion protection of AA7075 aluminum alloys, *Journal of Electrochemical Science and Engineering* **12(4)** (2022) 703-719. http://doi.org/10.5599/jese.1305

[58] J. J. Alba-Galvín, L. González-Rovira, F. J. Botana, M. Lekka, F. Andreatta, L. Fedrizzi, M. Bethencourt, Application of Commercial Surface Pretreatments on the Formation of Cerium Conversion Coating (CeCC) over High-Strength Aluminum Alloys 2024-T3 and 7075-T6, *Metals* **11(6)** (2021) 930. https://doi.org/10.3390/met11060930n

[59] C. E. Castano, W. G. Fahrenholtz, M. J. O'Keefe, Application of Commercial Surface Pretreatments on the Formation of Cerium Conversion Coating (CeCC) over High-Strength Aluminum Alloys 2024-T3 and 7075-T6, *Metal Oxides* (2020) 211-257. https://doi.org/10.1016/B978-0-12-815661-2.00006-2

[60] J. Espinoza-Vergara, S. Gad, C.P. Silva, M.A. Paez, Z. Jin, Y. Xiong, M. Azocar, N. Vejar,

C. Ramirez, X. Zhou, Covalent electrografting of aryl groups on AA2060-T8 surfaces, and their modification with Ce(4OHcin)$_3$ to incorporate additional anticorrosive activity, *Journal of Materials Research and Technology* **31** (2024) 3014-3024. https://doi.org/10.1016/j.jmrt.2024.07.009

[61] Z. Zhou, J. Liu, X. Meng, C. Zhou, Improved corrosion resistance and hydrophobic stability of sol–gel coatings by benzoxazine modification on aluminum alloys AA1060, *Journal of Coating Technology and Research* **21** (2024) 893-905. https://doi.org/10.1007/s11998-023-00858-4

[62] C. E. Castano, M. J. O'Keefe, W. G. Fahrenholtz, Cerium-based oxide coatings, *Current Opinion in Solid State and Materials Science* **19(2)** (2015) 69-76. https://doi.org/10.1016/j.cossms.2014.11.005

[63] R. Andreeva, E. Stoyanova, D. Stoychev, Study of the chemical formation of cerium oxide conversion layers on Aluminium - AD-3, *Journal of International Scientific Publications* **8** (2014) 751-759. https://www.scientific-publications.net/en/article/1000228/

[64] A. Simović, B. Milovanović, M. Etinski, L. Matović, J. B. Bajat, Innovative hybrid and bifunctional rare earth complexes as corrosion inhibitors for AA2024 Alloy: Electrochemical and surface analysis enhanced by DFT/MD simulation, *Applied Surface Science* **670** (2024) 160718. https://doi.org/10.1016/j.apsusc.2024.160718

[65] D. Wang, X. Yue, J. Zhao, P. Claesson, F. Zhang, J. Pan, Y. Shi, Enhancing adhesion and durability: A biomimetic approach with dopamine-modified lignin-polydimethylsiloxane coatings, *Corrosion Science* **236** (2024) 112274. https://doi.org/10.1016/j.corsci.2024.112274

[66] W. Pinc, S. Geng, M. O'Keefe, W. Fahrenholtz, T. O'Keefe, Effects of acid and alkaline based surface preparations on spray deposited cerium based conversion coatings on Al 2024-T3, *Applied Surface Science* **255** (2009) 4061-4065. https://doi.org/10.1016/j.apsusc.2008.10.110

[67] R. Andreeva, A. Tsanev, D. Stoychev, Effect of pre- and post-treatment operations of aluminum alloy Al-1050 protected by ceria conversion coatings, *Materials Today* **61** (2022) 1280-1286. http://doi.org/10.1016/j.matpr.2022.03.716

[68] I. I. Milošev, P. Rodič, The Effect of Surface Pretreatment of Aluminum Alloy 7075-T6 on the Subsequent Inhibition by Cerium(III) Acetate in Chloride-Containing Solution, *Journal of The Electrochemical Society* **169(1)** (2022) 011504. http://doi.org/10.1149/1945-7111/ac4933

[69] A. Covelo, S. Rodil, X.R. Nóvoa, M. Hernández, Development and characterization of sealed anodizing as a corrosion protection for AA2024-T3 in saline media, *Materials Today Communications* **31** (2022) 103468. https://doi.org/10.1016/j.mtcomm.2022.103468

[70] S. Kozhukharov, Ch. Girginov, Enhancement of the cerium oxide primer layers deposited on AA2024-T3 aircraft alloy by preliminary anodization, *Journal of Electrochemical Science and Engineering* **8(2)** (2018) 113-127. https://doi.org/10.5599/jese.478

[71] M. A. Iqbal, M. Fedel, Protective Cerium-Based Layered Double Hydroxides Thin Films Developed on Anodized AA6082, *Advanced Materials Science Engineering*, **2020** (2020) 5765393. https://doi.org/10.1155/2020/5785393

[72] L. Selegård, T. Poot, P. Eriksson, J. Palisaitis, P. O.Å. Persson, Z. Hu, K. Uvdal, In-situ growth of cerium nanoparticles for chrome-free, corrosion resistant anodic coatings, *Surface and Coatings Technology* **410** (2021) 126958. https://doi.org/10.1016/j.surfcoat.2021.126958

[73] M. A. Iqbal, H. Asghar, M. Fedel, Double doped cerium-based superhydrophobic layered double hydroxide protective films grown on anodic aluminium surface, *Journal of Alloys and Compounds* **844** (2020) 156112. https://doi.org/10.1016/j.jallcom.2020.156112

[74] O M Prada Ramirez, F. Martins Queiroz, M. A. Tunes, R. A. Antunes, C. L. Rodrigues, A. Lanzutti, S. Pogatscher, M-G. Olivier, H. G. De Melo, Tartaric-sulphuric acid anodized clad

AA2024-T3 post-treated in Ce-containing solutions at different temperatures: Corrosion behaviour and Ce ions distribution, *Applied Surface Science* **534** (2020) 147634. https://doi.org/10.1016/j.apsusc.2020.147634

[75] A. M. Brudzisz, D. Gizinski, W. J. Stepniowski, Incorporation of ions into nanostructured anodic oxides—mechanism and functionalities, *Molecules* **26(21)** (2021) 6378. http://doi.org/10.3390/molecules26216378

[76] M. Calovi, B. Furlan,V. Coroneo, O. Massidda, S. Rossi, Facile Route to Effective Antimicrobial Aluminum Oxide Layer Realized by Co-Deposition with Silver Nitrate, *Coatings* **12(1)** (2022) 28. https://doi.org/10.3390/coatings12010028

[77] O. M. Prada Ramirez, M. A. Tunes, M. M. Mennucci, M. Starykevich, Cristina Neves, M. G. S. Ferreira, S. Pogatscher, H. G. De Melo, Ce post-treatment for increased corrosion resistance of AA2024-T3 anodized in tartaric-sulfuric acid, *Corrosion Science* **204** (2022) 110371. https://doi.org/10.1016/j.corsci.2022.110371

[78] O M Prada Ramirez, F. Martins Queiroz, M. A. Tunes, R. A. Antunes, C. L. Rodrigues, A. Lanzutti, S. Pogatscher, M-G. Olivier, H. G. De Melo, Tartaric-sulphuric acid anodized clad AA2024-T3 post-treated in Ce-containing solutions at different temperatures: Corrosion behaviour and Ce ions distribution, *Applied Surface Science* **534** (2020) 147634. https://doi.org/10.1016/j.apsusc.2020.147634

[79] A. Kabir, H. Zhang, V. Esposito, Chapter 5 - Mass diffusion phenomena in cerium oxide, *Metal Oxides* (2020) 169-210. https://doi.org/10.1016/B978-0-12-815661-2.00005-0

[80] R.K. Harchegani, A.R. Riahi, Effect of Cerium Chloride on the Self-Corrosion and Discharge Activity of Aluminum Anode in Alkaline Aluminum-air Batteries, *Journal of The Electrochemical Society* **169(31)** (2022) 030542. https://doi.org/10.1016/j.surfcoat.2015.02.049

[81] P. Kumar, A. Kumar, R.C. Meena, R. Tomar, F. Chand, K. Asokan, Structural, morphological, electrical and dielectric properties of Mn doped CeO_2, *Journal of Alloys and Compounds* **672** (2016) 543-548. https://doi.org/10.1016/j.jallcom.2016.02.153

[82] S. Pundir, R. Priya, K. Singh, H. Kaur, P. Choudhary, A systematic study on synthesis of CeO_2 nanoparticles by various routes, A systematic study on synthesis of CeO_2 nanoparticles by various routes, *IOP Conference Series: Earth and Environmental Science* **1110** (2023) 012030. http://doi.org/10.1088/1755-1315/1110/1/012030

[83] M. A. K. Y. Shah, Y. Lu, N. Mushtaq, M. Y. B. Zhu, Unraveling the synergistic effect on ionic transport of ceria via the surface engineering for low-temperature ceramic fuel cells, *Applied Physics Letters* **122** (2023) 113902. https://doi.org/10.1063/5.0137303

[84] B. Fotovvat, M. Behzadnasab, S. M. Mirabedini, H. Eivaz Mohammadloo, Anti-corrosion performance and mechanical properties of epoxy coatings containing microcapsules filled with linseed oil and modified ceria nanoparticles, *Colloids and Surfaces A: Physicochemical and Engineering Aspects* **648** (2022) 129157. https://doi.org/10.1016/j.colsurfa.2022.129157

[85] O. M. Prada Ramirez, T. M. Kremmer, J. H. Marin, B. P. da Silva, M. Starykevich, M. A. Tunes, M. G. S. Ferreira, I. V. Aoki, R. A. Ando, S. Pogatscher, H. G. de Melo, Ce nanoparticles and sol-gel hybrid organic-inorganic coatings maximize corrosion protection in the anodized AA2024-T3, *Corrosion Science* **221** (2023) 111330. https://doi.org/10.1016/j.corsci.2023.111330

[86] G. Tsaneva, V. Kozhukharov, S. Kozhukharov, M. Ivanova, J. Gerwann, M. Schem, T. Schmidt, Functional nanocomposite coatings for corrosion protection of aluminum alloy and steel, *Journal of the University of Chemical Technology and Metallurgy* **43** (2008) 231-238. https://journal.uctm.edu/node/j2008-2/9_Kojukharov_231.pdf

[87] S. Portolesi, S. Kozhukharov, T. Haralanova, Ch. Girginov, Acidity adjustment of the solutions for coating deposition and further sealing by Lourier buffers, *Proceedings of University of Ruse* (Bulgaria) **61(10.1)** (2022) 68-73. https://conf.uni-ruse.bg/bg/docs/cp22/10.1/10.1-13.pdf

[88] S. Kozhukharov, C. Girginov, V. Lilova, P. Petkov, Innovative Applications of Cerium Oxide-Based Materials in Civil Engineering, Automation, and Energy Sectors", in*: Cerium - Chemistry, Technology, Geology, Soil Science and Economics,* M.T. Aide, Ed., Intechopen, 2024, 1-39. http://doi.org/10.5772/intechopen.1004168

[89] D. K. Heller, W. G. Fahrenholtz, M. J. O'Keefe, Effect of Phosphate Source on Post-Treatment of Cerium-Based Conversion Coatings on Al 2024-T3, *Journal of The Electrochemical Society* **156(11)** (2009) C400. http://doi.org/10.1149/1.3224005

[90] D. K. Heller, W. G. Fahrenholtz, M. J. O'Keefe, The effect of post-treatment time and temperature on cerium-based conversion coatings on Al 2024-T3, *Corrosion Science* **52** (2010) 360-368. https://doi.org/10.1016/j.corsci.2009.09.023

[91] R. Andreeva, E. Stoyanova, A. Tsanev, D. Stoychev, Influence of the Pre-Treatment and Post-Treatment Operations on the Surface Chemistry and Corrosion Behavior of Cerium-Based Conversion Coatings on Aluminum, *Current Advances in Chemistry and Biochemistry* **7** (2021) 1-28. http://doi.org/10.9734/bpi/cacb/v7/8429D

[92] R. Andreeva, E. Stoyanova, A. Tsanev, D. Stoychev, XPS characterisation of the influence of phosphate post-treatment of chemically deposited ceria protective layers on aluminum, *Comptes rendus de l'Acade'mie Bulgare des Sciences* **72(10)** (2019) 1336-1342. http://doi.org/10.7546/CRABS.2019.10.05

[93] R. Andreeva, D. Stoychev, Phosphate sealing improvement of the corrosion resistance of thin cerium oxides coatings electroless deposited on aluminium, *Journal of Physics, Conference Series* **2240** (2022) 012001. http://doi.org/10.1088/1742-6596/2240/1/012001

[94] D. I. Ivanova, Phosphating of zinc surfaces in zinc-calcium solutions, *Bulgarian Chemical Communications* **43** (2011) 54-59. http://www.bcc.bas.bg/bcc_volumes/Volume_43_Number_1_2011/Volume_43_Number_1_2011_PDF/2011-43-1_8.pdf

[95] V. Kovalenko, V. Kotok, Optimisation of the formation technology of tripolyphosphate coating on the mild steel, *Eastern-European Journal of Enterprise Technologies* **5 (6(113))** (2021) 73-78. http://doi.org/10.15587/1729-4061.2021.242409

[96] Y. Tumbaleva, D. Ivanova, L. Fachikov, Effect of the P_2O_5:NO_3 - ratio on the zinchosphate coating formation, *Journal of the University of Chemical Technology and Metallurgy* **46(4)** (2011) 357-362. https://journal.uctm.edu/node/j2011-4/3-Fachikov%20357-362.pdf

[97] E. Vlasova, V. Kovalenko, V. Kotok, S. Vlasov, K. Sukhyy, A study of the influence of additives on the process of formation and corrosive properties of tripolyphosphate coatings on steel, *Eastern-European Journal of Enterprise Technologies* **5(12-89)** (2017) 45-51. http://doi.org/10.15587/1729-4061.2017.111977

[98] V. S. Konovalova, V. E. Rumyantseva, Obtaining Red Phosphate Coatings on Steel at Room Temperature, *Engineering Proceedings* **56(1)** (2023) 54. https://doi.org/10.3390/ASEC2023-15378

[99] Ch. Girginov, S. Kozhukharov, M. Milanes, M. Machkova, Impact of the anodizing duration on the surface morphology and performance of A2024-T3 in a model corrosive medium, *Materials Chemistry and Physics* **198** (2017) 137-144. https://doi.org/10.1016/j.matchemphys.2017.05.049

[100] S. Kozhukharov, Ch. Girginov, S. Portolesi, A. Tsanev, V. Lilova, P. Petkov, Optimal current density for cathodic CeCC deposition on anodized AA2024-T3 aircraft alloy, *Journal of Applied Electrochemistry* **54** (2024) IN PRINT. https://doi.org/10.1007/s10800-024-02143-7

[101] S. Kozhukharov, Ch. Girginov, N. Boshkova, A. Tzanev, Impact of the final thermal sealing of combined zinc/cerium oxide protective coating primers formed on low carbon steel, *Journal of Electrochemical Science and Engineering* **12(4)** (2022) 685-701. http://doi.org/10.5599/jese.1297

[102] Ch. Girginov, S. Portolesi, S. Kozhukharov, A. Tsanev, E. Lilov, P. Petkov, Selection of appropriate electrochemical deposition regime for cerium conversion coating on anodized AA2024-T3 aircraft alloy, *Journal of Applied Electrochemistry* **54** (2024) 1171-1202. https://doi.org/10.1007/s10800-023-02012-9

[103] Y. Y. Lourier, Manual of Analytical Chemistry*, "Chemistry" Gov. ed.,* Moscow, 1979, 305-309. UDC 543-031 (in Russian).

[104] S. Kozhukharov, A. Dishliev, Ch. Girginov, Reproducibility of the surface characteristics of anodized aa2024-t3 aircraft alloy with deposited Ce-conversion coating, *Journal of Chemical Technology and Metallurgy* **57(2)** (2022) 353-360. https://journal.uctm.edu/node/j2022-2/18_21-68_No2_353-360.pdf

[105] S. V. Kozhukharov, Ch. A. Girginov, *Classical and Modern Methods for Corrosion Impact Rate Determination for Aluminium and Strengthened Aircraft Alloys. Fundamentals and Practical Applications*, in: *Phenomena and Theories in Corrosion Science. Methods of Prevention,* A. Gergely Ed., NOVA Sci. Publ., 2019, 3-150. ISBN 978-1-53615-252-4

[106] N. C. Nelson, Z. Wang, P. Naik, J. Sebastián Manzano, M. Pruski, I. I. Slowing, Phosphate modified ceria as a Brønsted acidic/redox multifunctional catalyst, *Journal of Materials Chemistry* **A-5** (2017) 4455-4466. https://doi.org/10.1039/C6TA08703E

[107] L. Chen, Y. Shen, Q. Wang, X. Wang, Y. Wang, B. Li, S. Li, S. Zhang, W. Li, Phosphate on ceria with controlled active sites distribution for wide temperature NH_3-SCR, *Journal of Hazardous Materials* **427** (2022) 128148. https://doi.org/10.1016/j.jhazmat.2021.128148

[108] X. Liu, K. Zhou, L. Wang, B. Wang, Y. Li, Oxygen vacancy clusters promoting reducibility and activity of ceria nanorods, *Journal of the American Chemical Society* **131** (2009) 3140-3141. https://doi.org/10.1021/ja808433d

[109] R. Schmitt, A. Nenning, O. Kraynis, R. Korobko, A. I. Frenkel, I. Lubomirsky, S. M. Haile, J. L. M. Rupp, A review of defect structure and chemistry in ceria and its solid solutions, *Chemical Society Reviews* **49** (2020) 554-592. https://doi.org/10.1039/C9CS00588A

[110] S. Baratov, E. Filonova, A. Ivanova, M. B. Hanif, M. Irshad, M. Z. Khan, M. Motola, S. Rauf, D. Medvedev, Current and further trajectories in designing functional materials for solid oxide electrochemical cells: A review of other reviews, *Journal of Energy Chemistry* **94** (2024) 302-331. https://doi.org/10.1016/j.jechem.2024.02.047

[111] J. A. Kilner, Defects and Conductivity in Ceria-based Oxides, *Chemical Letters* **37(10)** (2008) 1012-1015. https://doi.org/10.1246/cl.2008.1012

[112] A. Kabir, H. Zhang, V. Esposito, Mass diffusion phenomena in cerium oxide, *Metal Oxides* (2020) 169-210. https://doi.org/10.1016/B978-0-12-815661-2.00005-0

[113] H. Onoda, R. Tanaka, Synthesis of cerium phosphate white pigments from cerium carbonate for cosmetics, *Journal of Materials Research and Technology* **8(6)** (2019) 5524-5528. https://doi.org/10.1016/j.jmrt.2019.09.020

[114] H. Onoda, H. Muraki, Synthesis and Powder Properties of Cerium Phosphate White Pigments, *IOP Conference Series: Materials Science and Engineering* **613** (2019) 012045. https://doi.org/10.1088/1757-899X/613/1/012045

[115] T. Masui, H. Tategaki, S. Furukawa, N. Imanaka, Synthesis and characterization of new environmentally-friendly pigments based on cerium phosphate, *Journal of Ceramic Society of Japan* **112(12)** (2024) 646-649. https://doi.org/10.2109/jcersj.112.646

[116] G. El-Damrawi, F. Gharghar, R. Ramadan, More Insight on Structure of New Binary Cerium Borate Glasses, *New Journal of Glass and Ceramics* **8** (2018) 12-21. https://doi.org/.10.4236/njgc.2018.81002

[117] M. Ghosh, B. B. Nayak, One-pot synthesis and emission behavior of borate, mixed borate-oxide, and oxide-based luminescent materials, *Ceramics International* **50(13-B)** (2024) 23865-23875. https://doi.org/10.1016/j.ceramint.2024.04.115

[118] C. Mei, S. Deshmukh, J. Cronin, S. Cong, D. Chapman, N. Lazaris, L. Sampaleanu, U. Schacht, K. Drolet-Vives, M. Ore, S. Morin, B. Carpick, M. Balmer, M. Kirkitadze, Aluminum Phosphate Vaccine Adjuvant: Analysis of Composition and Size Using Off-Line and In-Line Tools, *Computational and Structural Biotechnology Journal* **17** (2019) 1184-1194. https://doi.org/10.1016/j.csbj.2019.08.003

[119] W. Zhang, W. Guan, Y. Wang, S. Lin, K. A. See, Enabling Al sacrificial anodes in tetrahydrofuran electrolytes for reductive electrosynthesis, *Chemical Science* **14** (2023) 13108-13118. https://doi.org/10.1039/D3SC04725C

[120] I. Latsunskyi, M. Kempiński, M. A. Jancelewicz, K. Załęski, S. Jurga, V. Smyntyna, Structural and XPS characterization of ALD Al_2O_3 coated porous silicon, *Vacuum* **113** (2015) 52-58. https://doi.org/10.1016/j.vacuum.2014.12.015

[121] Z. Ding, W. Xu, X. Zhang, Z. Liu, J. Shen, J. Liang, M. Jiang, X. Ren, Controllable Acid/Base Propriety of Sulfate Modified Mixed Metal Oxide Derived from Hydrotalcite for Synthesis of Propylene Carbonate, *Catalysts* **9** (2019) 470. https://doi.org/10.3390/catal9050470

[122] Y. Liu, J. Huang, J. B. Claypool, M. J. O'Keefe, Structure and Corrosion Behavior of Sputter Deposited Ce-Al-O Coating on Al 2024-T3 Alloy Substrates, *Journal of The Electrochemical Society* **163(5)** (2016) C198-C204. http://doi.org/10.1149/2.0671605jes

[123] K. P. Singh, A. Singh, N. Kumar, D. N. Tripathi, Morphological features, dielectric and thermal properties of epoxy-copper cobaltite nanocomposites: preparation and characterization, *Bulletin of Material Science* **43** (2020) 114. http://doi.org/10.1007/s12034-020-02092-9

[124] F. Lai, W. Yao, J. Li, Effect of B_2O_3 on Structure of CaO-Al_2O_3-SiO_2-TiO_2-B_2O_3 Glassy Systems, *ISIJ International* **60(8)** (2020) 1696-1601. http://doi.org/10.2355/isijinternational.ISIJINT-2019-679

[125] J. Cole, Z. Henderson, A. G. Thomas, C. Castle, A. J. Greer, C. Hardacre, M. Scardamaglia, A. Shavorskiy, K. L. Syres, In situ XPS of competitive CO_2/H_2O absorption in an ionic liquid, *Journal of Physics: Materials* **6** (2023) 045012. http://doi.org/10.1088/2515-7639/acfdcf

[126] R. Jonsson, O. Mihai, J. Woo, M. Skoglundh, E. Olsson, M. Berggrund, L. Olsson, Gas-Phase Phosphorous Poisoning of a Pt/Ba/Al_2O_3 NO_x Storage Catalyst, *Catalysts* **8(4)** (2018) 155. http://doi.org/10.3390/catal8040155

[127] Y. Zhou, G. Zheng, S. Cen, R. Liu, C. Tao, Leaching of phosphate ores with lower dissolution of metallic impurities: the dual role of sodium oleate, *RSC Advances* **13** (2023) 10600-10609. http://doi.org/10.1039/d3ra00897e

[128] R. Andreeva, D. Stoychev, Corrosion Characterisation of the Influence of Phosphate Post-Treatment of Chemically Deposited Ceria Protective Conversion Coatings on Aluminium, *Comptes rendus de l'Académie bulgare des Sciences* **74(9)** (2021) 1314-1323.

[129] H. Luhrs, R. X. Fischer, H. Schneider, Boron mullite: Formation and basic characterization, *Materials Research Bulletin* **47** (2012) 4031-4042. http://doi.org/10.1016/j.materresbull.2012.08.064

[130] M.González-Castaño, C. Cancellieri, X. Maeder, E. Hack, P. Schmutz, Enhancing the Insulating and Dielectric Properties of Barrier Anodic Al_2O_3 on High Purity Aluminum, *Applied Surface Science* **505** (2020) 144522. https://doi.org/10.1016/j.apsusc.2019.144522

[131] L. González-Rovira, L. González-Souto, P.J. Astola, C. Bravo-Benítez, F.J. Botana, Assessment of the Corrosion Resistance of Self-Ordered Anodic Aluminum Oxide (AAO) Obtained in Tartaric-Sulfuric Acid (TSA), *Surface and Coatings Technology* **399** (2020) 126131. https://doi.org/10.1016/j.surfcoat.2020.126131

[132] G. S. Frankel, J. R. Scully, C. V. Jahnesa, Repassivation of Pits in Aluminum Thin Films, *Journal of The Electrochemical Society* **143(6)** (1996) 1834-1840. https://doi.org/10.1149/1.1836912

[133] K.L. Moore, J.M. Sykes, P.S. Grant, An electrochemical study of repassivation of aluminium alloys with SEM examination of the pit interiors using resin replicas, *Corrosion Science* **50(11)** (2008) 3233-3240. https://doi.org/10.1016/j.corsci.2008.08.027

[134] S. Kozhukharov, V. Kozhukharov, M. Wittmar, M. Schem, M. Aslan, H. Caparrotti, M. Veith, Protective abilities of nanocomposite coatings containing Al_2O_3 nano-particles loaded by $CeCl_3$, *Progress in Organic Coatings* **71(2)** (2011) 198-205. https://doi.org/10.1016/j.porgcoat.2011.02.013

[135] M. P. Yunusov, Sh. Gulomov, K. A. Nasullayev, D. P. k. Turdiyeva, N. F. Isayeva, I. S. K. Abdurakhmanova, B. D. Mustafayev, D. Yu. Murzin, Hydrodesulfurization Catalysts from Aluminium-Containing Waste, *Catalysis Letters* **154** (2024) 4409-4421. https://doi.org/10.1007/s10562-024-04685-z